Kinetics of the Reaction of Propargyl Radical with Nitric Oxide

John D. DeSain, P. Y. Hung, Robert I. Thompson, Graham P. Glass,* Gustavo Scuseria,* and R. F. Curl*

Chemistry Department and Rice Quantum Institute, Rice University, Houston, Texas 77005

Received: November 30, 1999; In Final Form: February 16, 2000

The reaction between the propargyl radical (C_3H_3) and NO has been investigated as a function of temperature (195−473 K) and pressure (3−100 Torr) by using color center laser infrared kinetic spectroscopy. At room temperature and below, the reaction rate was found to depend strongly on the helium buffer gas pressure and, at any fixed buffer gas density, to decrease with increasing temperature. This behavior is consistent with the reaction occurring by termolecular addition to produce C_3H_3NO. Data collected over a wide pressure range at 195 and 296 K were fitted to a semiempirical model developed by Troe for reactions of this type. The structure and energetics of the adduct were explored by performing both B3LYP 6-311++G(2df,2pd) and G2 calculations. The enthalpy change, ΔH, for addition of NO to the CH end of propargyl was determined as −123 and −138 kJ/mol, respectively, by using these two methods. The calculations also showed that NO can add at the CH_2 end of propargyl but with a smaller binding energy. Estimates of the equilibrium constant for adduct formation, made using data obtained from these calculations, revealed that the addition reaction should shift from an equilibrium position strongly favoring the adduct to one strongly favoring free propargyl as the temperature is raised from 550 to 650 K. This temperature regime is higher than any of the temperatures reached experimentally.

Introduction

Reactions involving small hydrogen-deficient free radicals such as C_2H, C_2H_3, C_4H_5, and C_3H_3 are thought to be responsible for the formation of the first aromatic compounds produced during the combustion of aliphatic fuels. Aromatic ring formation is believed to occur as a result of these species reacting either with themselves or with various unsaturated hydrocarbons produced by pyrolysis, such as C_2H_2 and C_4H_2. Such reactions are extremely important because it is generally accepted that the formation of the first benzene ring is a necessary preliminary to the formation of both polyaromatic hydrocarbons and soot in flames.[1−5]

While the relative importance of various different mechanisms for soot formation is constantly being debated, recent studies[6] have suggested that the propargyl radical, C_3H_3, plays a major role in aromatic ring formation. Since propargyl is a resonantly stabilized species, it forms very weak bonds with stable molecules, and as a result, it reacts only slowly with molecular oxygen. Consequently, it may attain relatively high concentrations in flames. Indeed, in lightly sooting acetylene−oxygen flames, it has been shown[7] that propargyl is present at mole fractions as high as 10^{-3}. Westmoreland[7] has estimated that sufficient C_3H_3 is formed in such flames to account for aromatic ring formation.

Aromatic ring formation probably occurs as a result of the propargyl radical recombining with itself. This reaction is extremely fast, having a rate constant[8] between 0.5×10^{-10} and 1.2×10^{-10} cm^3 molecules^{-1} s^{-1} at 298 K. A number of different C_6H_6 isomers have been observed experimentally as stable products of the C_3H_3 recombination reaction,[9] and Melius and Miller[6] have determined that the initial adduct formed by recombination can rearrange to form benzene. A number of investigators[10−17] have concluded that this is probably the single most important reaction forming aromatic rings in combustion systems. However, it is worth noting that Westmoreland[7] found insufficient C_3H_3 to account for soot formation in 1,2-butadiene flames. Therefore, propargyl recombination is almost certainly not the *only* reaction creating aromatic rings in flames.

Despite the overall interest in propargyl by the combustion community, relatively little is known about reactions of C_3H_3. In addition to recombination, only reactions with molecular[18,8a] and atomic oxygen,[19] with $C_3H_3Cl_2$[8a] and $C_3H_3Br_2$,[8a] and with a number of stable hydrocarbon species[20] have been investigated directly. The reaction with O_2 exhibits[18,8a] quite interesting behavior. A termolecular addition reaction occurs at low temperatures (295−350 K). As the temperature is raised (380−430 K), equilibrium between the reactants and the $C_3H_3O_2$ adduct is established. As a result, the overall reaction rate decreases, and the propargyl radical is observed to decay to a quite measurable equilibrium concentration. However, when the temperature is increased above 500 K, the reaction rate increases, becomes pressure-independent, and exhibits a small, positive activation energy. In this later regime, H_2C_2O was identified as a major reaction product. Slagle and Gutman[18] interpreted this behavior as showing that a second irreversible decomposition channel for the adduct opens at temperatures above 430 K. The reaction of C_3H_3 with atomic oxygen has been shown to be very fast, occurring on almost every collision[19] between 295 and 750 K. However, its mechanism is not well-known because the primary products of the reaction have not been unambiguously identified. Propargyl reacts only slowly with saturated hydrocarbons. At 296 K, it has been found to be almost totally unreactive toward acetylene,[20] methane,[20] and a number of photolytic precursors (C_3H_3Cl and C_3H_3Br).[8b]

In this paper, an investigation of the reaction of propargyl with nitric oxide (NO) is reported. This reaction was chosen for study for two reasons. First, NO is a combustion species that is produced in low-temperature flames of almost all

10.1021/jp994227w CCC: $19.00
Published on Web 03/28/2000

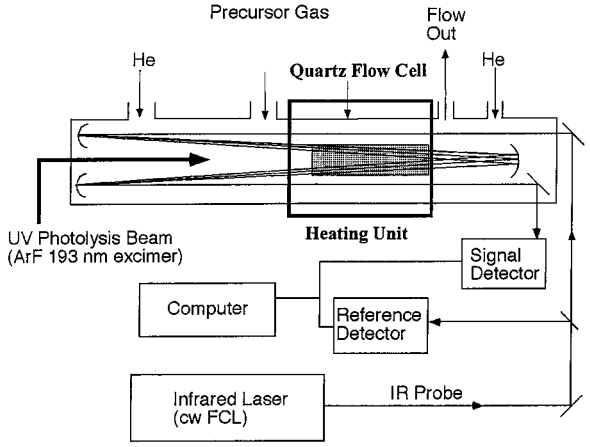

Figure 1. Infrared kinetic spectroscopy apparatus. The infrared probe beam and the excimer photolysis laser overlap in the shaded region.

nitrogen-containing fuels. In addition, it has been shown to react with several hydrocarbon radicals with rate constants 10−100 times greater than those measured for similar reactions with molecular oxygen.[21,22] Therefore, NO was considered to be a molecule that might play a practical role in retarding soot formation in flames. Second, it was hoped that the study of this reaction might shed some light on the manner in which the smallest of the resonantly stabilized hydrocarbon radicals reacts. Specifically, it was hoped that it might be possible to determine which end of the C_3H_3 radical is attacked by NO. Is the CH_2 end, which is normally assigned an unpaired electron when propargyl is represented as the acetylenic resonance hybrid ($^{\bullet}CH_2C{\equiv}CH$), attacked, or does reaction occur at the opposite end, which carries the unpaired electron when propargyl is represented as the allenic hybrid ($H_2C{=}C{=}CH^{\bullet}$)?

The titled reaction was studied by using infrared kinetic spectroscopy. The basis for the work reported here had been established in several previous studies. The acetylenic CH stretch of propargyl (the ν_1 band) had been thoroughly investigated,[22,23] resulting in an unambiguous assignment of the propargyl spectrum.

Experimental Section

High-resolution transient infrared absorption spectra of propargyl and a number of possible reaction products were observed by using a CW color center laser (Burleigh Instruments, FCl-20, Li:RbCl crystal, 2.6−3.2 μm), pumped by a krypton ion laser, as a tunable infrared light source. The computer scanning and control system of the FCL laser has been described previously.[24] Propargyl radicals were prepared in the flow cell by flash photolysis of a number of different precursors by using 193 nm pulses from an ArF excimer laser (Lambda-Physik EMG-MSC-103), and the propargyl concentration was monitored at 3314.703 cm^{-1} (P(12) of ν_1).[20,22]

An overview of the photolysis cell is shown Figure 1. Although the flow cell is 2 m in length, the IR and UV beams only overlapped in the shaded region, which is approximately 40 cm long. The relatively short overlap region results from the fact that the UV photolysis beam was angled upward as it traversed the flow cell, while the IR probe beam traveled back and forth (in a multipass White configuration) in the horizontal plane. Radicals generated by the excimer beam can *only* absorb light from the probe beam, and thus be detected, in the shaded intersection region. This configuration provided a very convenient arrangement for carrying out kinetics experiments at low or elevated temperature because only the shaded region of the apparatus needed to be heated or cooled. Therefore, it was not necessary to seal the windows to the flow tube in a manner that allowed them to withstand a wide variation in temperature.

To perform experiments at 195 K, the "overlap" region of the flow tube was packed in dry ice. To conduct experiments at elevated temperatures, an oven was placed over the flow cell, as described previously.[25] The temperature was monitored by two thermocouples (type K, Alumel Omega), one placed at the center of the IR−UV overlap region between the ceramic heater and the quartz flow cell and the other near the end of the IR−UV overlap region. In this study, the temperature gradient between the center and the end of the overlap region was minimized by differentially heating different sections of the oven. This procedure reduced the measured temperature difference between the two thermocouples to less than 2 °C.

Calculations made by using standard heat transport theory indicated that the temperature of the gas within the flow cell should have been almost the same as the temperature of the cell tube wall. To check that this was the case, the line width of an isolated NH_2 line, produced in the overlap region by the flash photolysis of NH_3 at 193 nm, was measured. The temperature was estimated by assuming the line to be Doppler broadened. For such a line, the line width, $\Delta\nu_D$, is related to the temperature, T, by the equation

$$\Delta\nu_D = 2\nu_0\left(\frac{2kT\ln(2)}{mc^2}\right)^{1/2} \quad (1)$$

where ν_0 is the peak frequency of the absorption line and m is the mass of the molecule being observed.

The measurements were made by observing a NH_2 transition ($F_1\ 6_{42} \leftarrow 5_{33}$) at 3428.8077 cm^{-1}.[26] The total pressure in the flow cell was adjusted to approximately 10 Torr with about 9 mTorr of this being NH_3 while the rest was He carrier gas. A series of four measurements at room temperature gave an apparent average gas temperature of 322 ± 10 K. Presumably, the neglect of residual pressure broadening resulted in a systematically high temperature being estimated by using eq 1. A similar set of four measurements made when the flow cell was heated to a wall temperature of 473 K (determined by using the thermocouple) gave an average gas temperature of 471 ± 10 K. Considering the low precision of this type of measurement, this degree of agreement was considered to be satisfactory, especially since the relative effect of pressure broadening should have been be significantly less at 473 K than at 296 K.

Initially, C_3H_3 was produced by 193 nm photolysis of C_3H_3X (X being either Br or Cl). Both materials were obtained from Aldrich. C_3H_3Cl (98%) was used without further purification, but C_3H_3Br (80% in toluene) was purified by vacuum distillation. The concentration of propargyl was followed by monitoring an absorption at 3314.703 cm^{-1} (P(12) of ν_1 [22]). At room temperature and below, the absorption−time traces obtained when using these two precursors appeared to be entirely normal. The absorption increased immediately following the flash and then decreased smoothly as C_3H_3 was removed by reaction, asymptotically approaching the original baseline at longer reaction times. However, at elevated temperatures, a different behavior was observed. Instead of approaching the original baseline, the absorption decayed to a new baseline that was offset from the original one in the direction of decreased absorption. In an effort to understand this behavior, a number of experiments were performed with the IR probe laser tuned slightly away from the frequency at which C_3H_3 absorbs. A typical absorption−time trace obtained from one of these

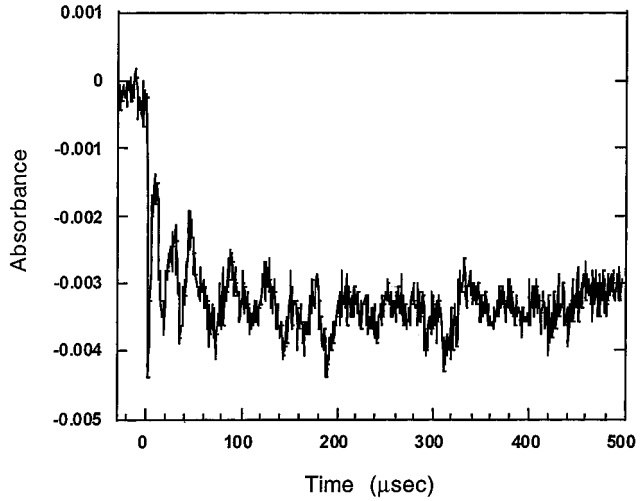

Figure 2. Transient signal obtained at 473 K upon photolysis of propargyl bromide with infrared laser tuned off any propargyl radical absorption near propargyl P(12) line. There is a clear baseline offset, believed to be caused by removal by photolysis of background absorption by propargyl bromide.

experiments is shown in Figure 2. As can be seen, a sudden shift in the baseline (in the direction of decreased absorption) occurred immediately following the UV flash. This baseline shift was attributed to an underlying absorption of the precursor. Since the flash removes some of the precursor, the underlying absorption logically should decrease, exactly as observed in Figure 2. The shift occurred over a broad frequency range and appeared to affect much of the C_3H_3 ν_1 fundamental wavelength region. The shift was more pronounced at higher temperatures because of decreased absorption by C_3H_3 as the result of decreased population in the lower state and because the underlying background absorption increased. We believe that the background absorption increased because we were positioned near the edge of an underlying feature that further broadened as the temperature increased.

In an attempt to alleviate the problem of baseline shift, which introduced a significant element of uncertainty into all of our higher temperature rate constant determinations, two other C_3H_3 precursors, which do not absorb so strongly in the acetylenic C−H stretch region of the infrared, were explored. When allene was photolyzed at 193 nm, significant concentrations of propargyl were produced. However, a baseline shift in the opposite direction (more absorption) was observed. Since the baseline shift gradually increased over a time period of 100 μs or so, this offset was attributed to the growth of one or more absorbing reaction products. 1,5-Hexadiyne (synthesized by a standard laboratory preparation[27]) was also used as a precursor. Unfortunately, baseline shifts were not entirely eliminated by using this compound. However, they were less severe than those experienced using C_3H_3X. Therefore, this precursor was used in all experiments performed at 473 K. At this higher temperature, two consecutive absorbance−time traces were recorded for each decay, one with the IR probe tuned to the peak frequency of the C_3H_3 absorption and the other with the probe tuned away from the C_3H_3 absorption. The latter trace was then subtracted from the former before further data analysis was performed.

The gases used in the investigation were purchased from Trigas with purities as follows: He (99.999%), CO_2 (99.5%), and SF_6 (99.8%). NO (99%) was purified by flowing it at pressures slightly above 1 atm through a copper coil immersed in a dry ice/methanol bath. It was then premixed with He before being introduced into the flow cell. The flow rate of NO was measured by using a MKS 200 sccm flow controller. The total pressure of the flow cell was varied between 2 and 100 Torr, with helium being the dominant species present.

Observations

C_3H_3 + NO Rate Constant. In this study, NO was always added to the system in sufficient excess to maintain its concentration at a value that was not sensibly diminished by reaction with C_3H_3. Under these conditions, C_3H_3 was removed primarily by the following reaction, which is effectively first order, with a rate constant k_{eff} equal to k_2[NO].

$$C_3H_3 + NO \rightarrow \text{products} \tag{2}$$

To a lesser extent, propargyl was also removed by radical recombination:

$$C_3H_3 + C_3H_3 \rightarrow \text{products} \tag{3}$$

In these circumstances, the overall rate equation for C_3H_3 loss can be written as a sum of two terms, one first order and the other second order, with respect to C_3H_3.

$$\frac{d[C_3H_3]}{dt} = -k_{eff}[C_3H_3] - k_3[C_3H_3]^2 \tag{4}$$

In most standard absorption experiments, the concentration of C_3H_3 would have been estimated directly from the measured value of the base e absorbance, A, which is related to $[C_3H_3]$ by the equation

$$A = \sigma_{IR} L [C_3H_3] \tag{5}$$

where L is the absorption path length and σ_{IR} is the peak infrared absorption cross section. Then the $[C_3H_3]$/time profile would have been fitted to the integrated form of eq 4 to yield a value for the effective first-order rate constant k_{eff}.

However, in these experiments, the path length of the IR probe was not well-known because the exact geometry of the overlap region was difficult to determine. Therefore, it turned out to be more convenient to recast eq 4 in terms of the measurable quantity A before integrating[21] to obtain

$$A = \frac{A_0 \exp(-k_{eff}t)}{(2k_3/S)(A_0/k_{eff})(1 - \exp(-k_{eff}t)) + 1} \tag{6}$$

In the above equation, $S = \sigma_{IR}L$ and A_0 is the initial absorbance of C_3H_3.

In the present study, the pseudo-first-order rate constant k_{eff} (at particular values of [NO], total pressure, and temperature) was determined in the following manner. First, a value for (k_3/S) was obtained by making an independent series of measurements in the *absence* of NO. Then, by use of this value, absorbance−time traces measured in the presence of a specific partial pressure of NO were fitted to eq 6 to obtain k_{eff}.

In the *absence* of NO, propargyl is removed solely by reaction 3, and the integrated form of the rate equation for this second-order process is well-known. The equation can be readily transformed into the following expression by substituting for $[C_3H_3]$ using eq 5:

$$A = \frac{A_0}{1 + (2k_3/S)A_0 t} \tag{7}$$

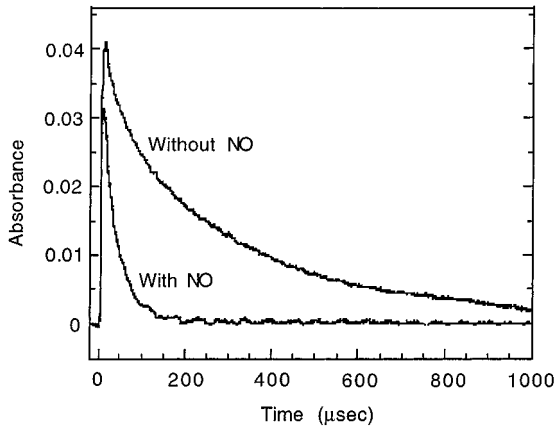

Figure 3. Decay of the propargyl signal without NO and in the presence of 114 mTorr of NO at a total pressure of 6.2 Torr at 296 K.

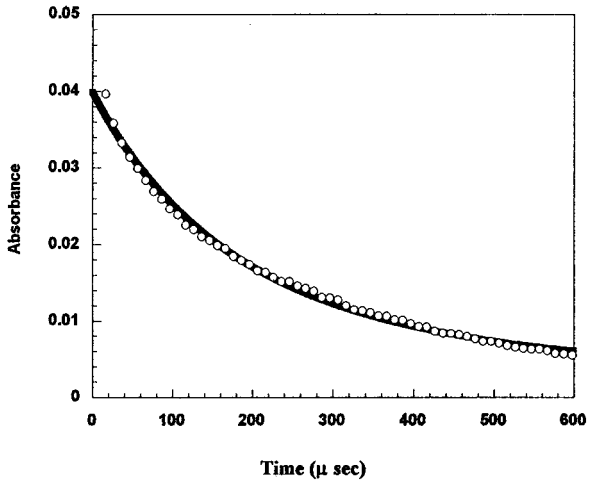

Figure 4. Typical second-order decay fit of the propargyl signal of Figure 6 in the absence of NO. From this fit the quantity k_3/S is found to be 30 440 s^{-1}.

In practice, k_3/S was determine prior to and after every series of rate constant measurements by fitting absorbance−time traces obtained in the *absence* of NO to eq 7. The average of these two values of k_3/S was then used as a fixed constant to fit experimental data to eq 6.

Absorbance−time traces for propargyl obtained at 296 K and at a total pressure of 6.2 Torr are shown in Figure 3. The upper trace was recorded in the absence of NO, while the lower trace was recorded in the presence of 114 mTorr of NO. Under these conditions, the decay of propargyl is 6−7 times faster in the presence of NO than in its absence. This situation was typical for most of the measurements reported here. Figure 4 shows a typical second-order fit of the decay of the propargyl signal obtained with no NO present, while Figure 5 shows a fit of the propargyl signal to eq 6 with NO present. Values of k_3/S were determined from plots similar to that shown in Figure 4, and values of k_{eff} were determined from plots similar to that shown in Figure 5.

At any given temperature and pressure, the rate constant k_2 was determined by plotting k_{eff} versus [NO]. Such a plot is shown in Figure 6. Values of k_2, estimated from the slope of k_{eff} versus [NO], are listed in Table 1 for a number of different pressures at three temperatures. Each individual measurement listed in this table was obtained by analyzing 8−10 different decay curves, each recorded in the presence of a different concentration of NO.

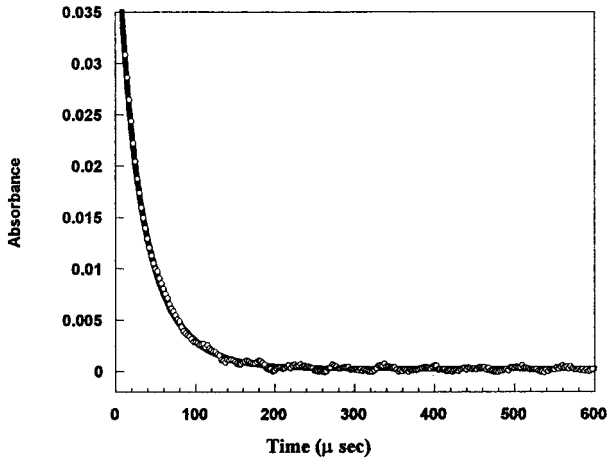

Figure 5. Fit of the decay of the propargyl signal in the presence of NO of Figure 6 to a combined first- plus second-order fit. The value of k_3/S was fixed to 30 440 s^{-1}, resulting in a first-order decay constant of 13 119 s^{-1}.

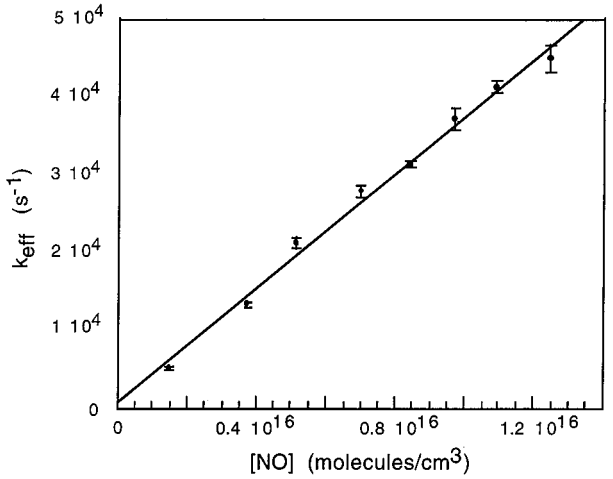

Figure 6. k_{eff} vs [NO] for the reaction C_3H_3 + NO at 6.2 Torr total pressure and 296 K. The linear fit corresponds to $k = (3.5 \pm 0.2) \times 10^{-12}$ cm^3 s^{-1}.

Pressure Dependence of the Reaction Rate. Figure 7 shows the pressure dependence of the second-order rate constant k_2 determined at 195, 296, and 473 K. The strong pressure dependence of the rate constant observed at the two lower temperatures and its negative temperature dependence suggest that reaction in this temperature regime occurs primarily by termolecular addition. Such processes are frequently described in terms of a Lindemann−Hinshelwood (L−H) mechanism.

$$C_3H_3 + NO \leftrightarrows C_3H_3NO^* \quad (8)$$

$$C_3H_3NO^* + M \leftrightarrows C_3H_3NO + M \quad (9)$$

In this mechanism, M is any species that can remove energy from the "hot" $C_3H_3NO^*$ complex. At low temperatures, the endothemic reaction (−9) is extremely slow and can be ignored. Then the rate of loss of C_3H_3 can be estimated by using the steady-state approximation for $[C_3H_3NO^*]$ as

$$-\frac{d[C_3H_3]}{dt} = k[C_3H_3][NO] = \frac{k_8k_9[C_3H_3][NO][M]}{k_{-8} + k_9[M]} \quad (10)$$

and the pressure-dependent second-order rate overall constant k can be written as

TABLE 1: Pressure Dependenceof the C_3H_3 + NO Reaction Rates at 195, 296, and 473 K

temp, K	pressure, Torr	rate, cm^3 $molecule^{-1}$ s^{-1} × 10^{-11}
195	2.2	0.668 ± 0.174
195	3.2	0.798 ± 0.044
195	4.5	0.981 ± 0.044
195	6.2	1.006 ± 0.058
195	12	1.004 ± 0.041
195	18	1.232 ± 0.057
195	20	1.041 ± 0.039
195	26	1.053 ± 0.176
195	32	1.325 ± 0.046
195	32	1.511 ± 0.062
195	40	1.354 ± 0.046
195	44	1.298 ± 0.079
296	3	0.249 ± 0.033
296	3	0.275 ± 0.021
296	6.2	0.345 ± 0.021
296	12	0.427 ± 0.017
296	18	0.546 ± 0.019
296	24	0.556 ± 0.010
296	24	0.515 ± 0.011
296	50	0.712 ± 0.024
296	75	0.880 ± 0.030
296	100	0.820 ± 0.015
473	6.2	0.107 ± 0.019
473	18	0.121 ± 0.010
473	30	0.133 ± 0.009

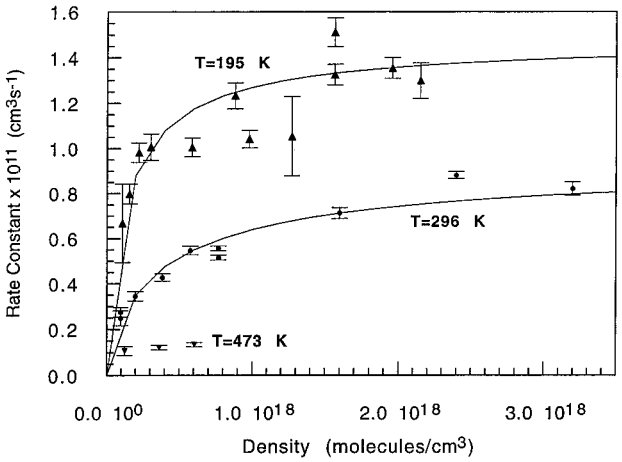

Figure 7. Dependence on He buffer gas density of the rate constant of the C_3H_3 + NO reaction at three different temperatures: 195 (▲), 296 (◇), and 473 (●) K.

$$k = \frac{k_8 k_9[\mathrm{M}]}{k_{-8} + k_9[\mathrm{M}]} \tag{11}$$

The rate constants displayed in Figure 7 vary with pressure in a manner that is consistent with eq 11. However, all of the experimental measurements lie within the "falloff" region. Unfortunately, it was not possible to make rate measurements at higher or lower pressures. At higher pressures, pressure broadening of the infrared absorption lines dramatically reduced our sensitivity, while at lower pressures, diffusion out of the probe beam reduced the time during which reliable measurements could be made. In addition, as the total pressure was reduced, the mole fractions of both NO and C_3H_3Cl necessarily increased. This causes difficulties in interpreting data obtained at pressures below 3 Torr because both of these species are more efficient than helium in removing energy from the excited adduct.

In an effort to extrapolate our experimental rate data to obtain the limiting high- and low-pressure rate coefficients k_∞ and k_0, we attempted to fit the data obtained at dry ice temperature and room temperature to the following equation, suggested by Troe.[28,29]

TABLE 2: Parameters of the Troe Fit for the C_3H_3 + NO Reaction at 195 and 296 K with *F* Fixed at 0.4 and 0.8 and $N = 1$

reaction	temp, K	$k_\infty \times 10^{11}$ cm^3 $molecule^{-1}$ s^{-1}	$k_0/[\mathrm{M}] \times 10^{29}$ cm^6 $molecule^{-2}$ s^{-1}	F^{SC}_{cent}
C_3H_3 + NO	195	1.69 ± 0.07	61.96 ± 12.16	0.4
C_3H_3 + NO	195	1.53 ± 0.06	17.83 ± 3.33	0.8
C_3H_3 + NO	296	1.12 ± 0.07	11.80 ± 1.68	0.4
C_3H_3 + NO	296	0.97 ± 0.05	3.80 ± 0.51	0.8
C_3H_5 + NO	296	1.35 ± 0.03	4.0 ± 1.7	*a*

[a] Not available.

$$k/k_\infty = \frac{k_0/k_\infty}{1 + k_0/k_\infty} F = F_{\mathrm{L-H}} F \tag{12}$$

In this equation, $k_0 = (k_8 k_9/k_{-8})[\mathrm{M}]$, $k_\infty = k_8$, the general broadening factor F is given by

$$\log F = \frac{\log F_{\mathrm{cent}}}{1 + [\log(k_0/k_\infty)]^2} \tag{13}$$

and the expression in parentheses is associated with the classic Lindemann−Hinshelwood term $F_{\mathrm{L-H}}$.[30] Equations 12 and 13 were suggested by Troe in order to approximate, with tolerable precision, the falloff behavior actually found in experimental measurements of the pressure-dependent rate constant k. The general broadening factor F was introduced by Troe to correct the original Lindemann−Hinshelwood expression both for neglect of the energy dependence of the microcanonical dissociation rate coefficients that contribute to k_{-8} and for the occurrence of weak collisions, which affect reactions forming and removing the excited adduct.

When we attempted to fit our data to eq 12, we found that the parameters k_∞, k_0 and F_{cent} were poorly determined. However, since Troe found that values of F_{cent} typically lie in the range 0.4−1 for systems of the type studied here, we fitted the rate constants measured at 195 and 296 K to eq 12 with F_{cent} fixed at both 0.4 and 0.8. The best fits obtained with F_{cent} fixed at 0.8 are shown in Figure 7. A similar quality of fit was obtained with F_{cent} fixed at 0.4. The resulting values of k_0 and k_∞ are listed in Table 2, together with parameters determined by Tulloch et al.[31] for the reaction of the allyl radical (C_3H_5) with NO. Since the experimental data were obtained relatively close to the high-pressure limit, k_∞ is quite well defined using both values of F_{cent}, but the error in k_0 is substantial.

Structure and Energy of C_3H_3NO. To determine the structure and energy of the C_3H_3NO adduct, quantum chemical calculations were performed at several levels of theory using[32] Gaussian 94 on an IBM workstation. Two general computational methods were employed: B3LYP using the 6-311++G(2df,2pd) basis set, and the G2 method of Curtiss, Raghavachari, Trucks, and Pople.

As a result of the calculations, two different stable isomers of C_3H_3NO were identified: one formed by addition of NO at the CH_2 end of propargyl (heads) and the other by addition of NO at the CH end (tails). Both computational methods identified the latter isomer as the most stable one.

The geometric structures of the two stable isomers from the B3LYP calculation are shown in Figure 8 (the G2 calculation structures were optimized at the MP2 level). Both structures are planar except for the CH_2 hydrogens; however, the ONH_2C_3H adduct has a gauche conformer 2.4 kJ/mol (G2)

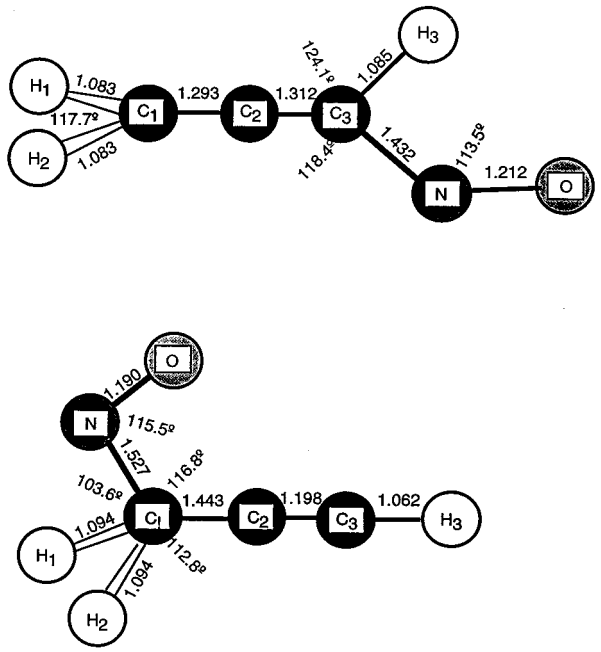

Figure 8. Equilibrium structures of the two adducts of propargyl with NO as calculated at the B3LYP 6-311G(2df,2pd) level. As noted in the text, the $C_1C_2C_3$ bond angles are nearly 180°, and the $C_2C_3H_3$ bond angle of the ONH_2C_3H adduct (lower figure) is also nearly 180°.

above the planar form in which the NO group is twisted out of the NC_1C_2 plane by 131.9° (B3LYP), resulting in a double-minimum torsional potential. For all structures the CCC angle was very close to 180° (178.9° for the H_2C_3HNO adduct and 179.8° for the ONH_2C_3H heavy atom planar adduct in B3LYP), and the $C_2C_3H_3$ angle of *gauche* ONH_2C_3H is 179.6° (B3LYP). Table 3 lists the enthalpies and entropies of C−NO bond formation for both structures. As can be seen from this table, the discrepancy in the heat of reaction to form the more strongly bound adduct (with addition at the CH end of propargyl) between the B3LYP and G2 estimates was 15.3 kJ/mol, a value that is significant but still acceptable. However, when the adduct was formed by addition of NO at the CH_2 end, the discrepancy between the two calculations increased to 35.9 kJ/mol. This discrepancy is consistent with the known[33] inability of B3LYP (and other DFT methods) to describe the relative stability of allene (C=C=C) vs propyne (C−C≡C).

Possible barriers to adduct formation were explored in a series of calculations made using the B3LYP 6-311++G(2df,2pd) method. In these calculations, the C−N bond distance was allowed to systematically increase from that found in the stable adduct configuration, and a search was made for structures containing an imaginary frequency in the reaction coordinate. No barrier was found in the formation path of either adduct. However, it is unlikely that small barriers (<3 kJ/mol) would have been discerned using this technique. No effort was made to find a reaction path leading from the adduct to any product channel.

Adduct formation in the related $C_3H_3 + O_2$ system was also explored at the B3LYP 6-311++G(2df,2pd) level. The heat of reaction for addition of O_2 to the CH end of propargyl was −76.8 kJ/mol. This value is consistent with that determined experimentally[18] (−79 ± 6 kJ/mol). The heat of reaction obtained for addition of O_2 to the other end of the radical was −50.4 kJ/mol.

The G2 zero-point energies and B3LYP vibrational frequencies and rotational constants were used to calculate the equilibrium constants for the formation of both the heads and the tails adducts. Then the fraction of each adduct at equilibrium in the presence of a fixed partial pressure of 200 mTorr of NO was calculated *assuming that only that adduct forms*. The results of these calculations are depicted in Figure 9. For the ONH_2C_3H adducts, the two gauche enantiomers and planar forms are lumped together in Figure 9 and considered to be a single species. As can be seen, the equilibrium position of both adducts is projected to shift dramatically as the temperature is raised. Below 600 K, the formation of the stronger adduct is overwhelmingly favored, but as the temperature is increased above 600 K, more and more free propargyl should be found in the equilibrium mixture. Unfortunately, at temperatures above 500 K, severe problems with a sloping unstable baseline and poor *S/N* made kinetics measurements unreliable.

TABLE 3: Quantum Chemistry Calculation Results of C_3H_3 Adduct Formation with NO[a]

reaction	$\Delta H°_{rxn}$ (kJ mol^{-1})	$\Delta S°_{rxn}$ (J mol^{-1} K^{-1})
$C_3H_3 + NO \rightarrow H_2C_3HNO$ (B3LYP)	−123.2	−158.9
$C_3H_3 + NO \rightarrow H_2C_3HNO$ (G2)	−138.5	
$C_3H_3 + NO \rightarrow ONH_2C_3H$(pl) (B3LYP)	−81.8	−153.6
$C_3H_3 + NO \rightarrow ONH_2C_3H$(pl) (G2)	−117.7	
$C_3H_3 + NO \rightarrow ONH_2C_3H$(g) (B3LYP)	−78.6	−144.1[c]
$C_3H_3 + NO \rightarrow ONH_2C_3H$(g) (G2)	−115.2	
$C_3H_3 + O_2 \rightarrow H_2C_3HO_2$ (B3LYP)	−76.8	−147.5
$C_3H_3 + O_2 \rightarrow H_2C_3HO_2$ (obsd)[b]	−79 ± 6	−131 ± 12
$C_3H_3 + O_2 \rightarrow O_2H_2C_3H$(g) (B3LYP)	−50.4	−142.2

[a] Thermodynamic quantities at 298 K. [b] Reference 18. [c] R ln 2 has been added to take into account the fact that the gauche form consists of two enantiomers.

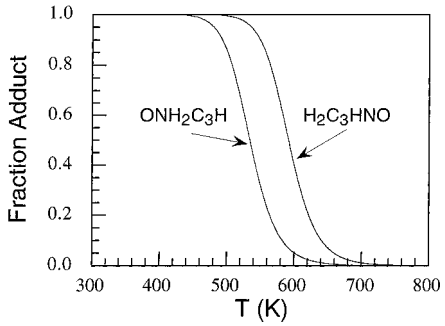

Figure 9. Ratio of the equilibrium concentration of propargyl−NO adducts to initial C_3H_3 concentration *assuming the other adduct is not present* plotted as a function of temperature. NO partial pressure is 200 mTorr.

Discussion

At room temperature and below the reaction between the propargyl radical and NO occurs by a mechanism that involves reversible addition. This can be inferred from the pressure dependence of the second-order rate constant and from its negative temperature dependence. Similar mechanisms have been proposed[31,34] for the reaction of several other hydrogen-deficient radicals with NO.

As is apparent from Figure 7, the termolecular addition reaction forming C_3H_3NO is in the falloff region in the pressure range covered by this study. In view of this, a factorization method suggested by Troe was used to extrapolate the experimental data to higher and lower pressures. The limiting high-pressure rate constants that were obtained by using this method are quite consistent with those reported by Tulloch et al.[31] for the related $C_3H_5 + NO$ system. However, the limiting third-order low-pressure rate constants are poorly determined and

depend strongly on the value of F_{cent} chosen to fit the experimental data.

Theoretical calculations, performed using both B3LYP and G2 methods, identified at least two stable addition products. The most strongly bound of these two adducts is an allenic structure formed by adding NO to the CH end of the propargyl radical. The other, less stable, structure is formed by adding NO to the CH_2 end of the radical. Generally, conjugated hydrocarbon radicals can be attacked at more than one site. In this sense their behavior is quite different from that of alkyl or vinyl radicals, and this difference must be taken into account when calculating rates or considering reaction mechanisms that involve these species.

Equilibrium geometries, heats of formation, and standard molar entropies were estimated for both C_3H_3NO adducts. Calculations, made using equilibrium constants determined from these estimates, suggest that equilibrium between the more stable adduct and free propargyl should be observable at temperatures between 500 and 650 K.

Possible Effects of the CH_2 End Adduct on the Rate. Both the B3LYP and G2 calculations indicate that the bonding of NO to the CH_2 end of propargyl is probably somewhat stronger than the bonding of O_2 to the CH end of propargyl. The reaction rate to form an adduct is clearly rapid for O_2. In addition, as noted above, the B3LYP calculations found no barrier to adduct formation for attack by NO at the CH_2 end of propargyl. Does adduct formation at the CH_2 end contribute to the reaction rate?

Because the bond strength of the CH end adduct is much greater than the bond strength of the CH_2 adduct, the equilibrium concentration of the CH_2 end adduct is always small (at an NO pressure of 0.2 Torr it reaches a maximum fraction of 0.05 near 550 K). However, this by itself does not mean that the contribution of CH_2 end adduct formation to the overall reaction rate is also negligible. At low temperatures, both adducts might form initially in nearly equal rates, and then the weaker adduct could slowly dissociate back to reactants eventually being converted to the strong adduct. In the absence of significant propargyl−propargyl recombination, such a kinetic mechanism would result in a biexponential C_3H_3 decay profile. We did not observe any clearly biexponential time profiles at any of the three temperatures investigated. However, at low temperatures, the slow component of the biexponential would have a very low amplitude because the weak adduct equilibrium would be strongly in the direction of adduct. At the highest temperature we report, 473 K, we are at the low-temperature edge of the temperature regime where the dissociation rate of the weaker adduct is comparable to and, eventually as the temperature increases, larger than its formation rate. Thus, at only slightly higher temperatures, it is likely that redissociation of the weak adduct will be relatively rapid (see Figure 9). Could this lead to a recognizable biexponential decay profile?

There is a simple strong argument against significant contributions of the weaker adduct to the rate at least at low pressure. There are two Lindemann−Hinshelwood processes taking place, one producing the H_2C_3HNO adduct and the other producing the ONH_2C_3H product. Suppose the former has the Lindemann−Hinshelwood rates k_8, k_{-8}, and k_9 from the reaction scheme described above and the latter has the rates k'_8, k'_{-8}, k'_9. There is no apparent reason k'_8 should not be about the same as k_8, and k'_9 should not be about the same as k_9; however, there is a good reason k'_{-8} should be greater than k_{-8}. Consider the dissociation of the nascent adducts before collisional stabilization as a unimolecular decay process, and apply simple RRK theory to this dissociation. The RRK formula is[35]

$$k_{-8}(E) = \nu\left(\frac{E - E_0}{E}\right)^{s-1} = \nu\left(\frac{E_T}{E_0 + E_T}\right)^{s-1} \quad (14)$$

where $k(E)$ is the rate of dissociation at energy E above the minimum, ν is vibrational frequency of the critical oscillator, E_0 is the dissociation threshold energy, s is the total number of effective oscillators, and E_T is the available thermal energy (we omit the rotational energy of the colliding pair). This classical formula is only approximately correct but is sufficient to convey the concepts. $E_0(H_2C_3HNO) = D_0(H_2C_3HNO)$ and $E_0(ONH_2C_3H) = D_0(ONH_2C_3H)$, where the D_0's are the bond dissociation energies. E_T is the same for the two adducts so that assuming the critical oscillator frequencies are the same,

$$\frac{k'_{-8}}{k_{-8}} \approx \left(\frac{D_0(H_2C_3HNO) + E_T}{D_0(ONH_2C_3H) + E_T}\right)^{s-1} \quad (15)$$

with $s - 1 = 3N - 7 = 17$. The G2 results give about a factor of 13 at 473 K for the ratio k'_{-8}/k_{-8}. The use of all the oscillators probably overestimates this ratio, but the above argument clearly shows that k'_{-8} is greater than k_{-8}. In the low-pressure limit where

$$k_{eff} = \frac{k_8 k_9}{k_{-8}}[M] \quad (16)$$

the weak adduct reaction rate should be substantially less than the strong adduct reaction rate. Simulations indicate that it would very hard to discern a biexponential component to the decay for a ratio (15) as small as 5. In the high-pressure limit, k_{-8} disappears from the Hinshelwood−Lindemann rate constant, the overall rate constant becomes $(k_8 + k'_8)$, and the weak adduct may contribute to the reaction rate. The experiments reported here are far from this high-pressure limit.

Thus, the question posed at the beginning of this paper concerning whether both radical reaction reaction sites contribute to the overall reaction has a partial theoretical answer. If the reaction under consideration is strictly adduct formation, the weaker binding site should contribute little at low pressures but could contribute significantly at high pressures.

Acknowledgment. This work was supported by the Department of Energy and the Robert A. Welch Foundation. We thank David Barry and Graham Scott for preparing a sample of 1,5-hexadiyne.

References and Notes

(1) Frenklach, M.; Clary, D. W.; Gardiner, W. C.; Stein, S. E. *Symp. (Int.) Combust., 20th* **1985**, 887.
(2) Warnatz, T.; Bockhorn, H.; Moser, A.; Wenz, H. W. *Symp. (Int.) Combust., 19th* **1983**, 197.
(3) Bittner, J. D.; Howard, J. B. *Symp. (Int.) Combust., 18th* **1981**, 1105.
(4) Homann, K.; Wagner, H. G. *Symp. (Int.) Combust., 11th* **1967**, 371.
(5) Bockhorn, H.; Fettig, F.; Wenz, H. W. *Ber. Bunsen-Ges. Phys. Chem.* **1983**, *87*, 1067.
(6) Miller, J. A.; Melius, C. F. *Combust. Flame* **1992**, *91*, 21.
(7) Westmoreland, P. R.; Dean, A. M.; Howard, J. B.; Longwell, J. P. *J. Phys. Chem.* **1989**, *93*, 8171.
(8) (a) Atkinson, D. B.; Hudgens, J. W. *J. Phys. Chem.* **1999**, *103*, 4242. (b) Morter, C. L.; Farhat, S. K.; Adamson, J. D.; Glass, G. P.; Curl, R. F. *J. Phys. Chem.* **1994**, *98*, 7029.
(9) Alkemade, U.; Homann, K. H. *Z. Phys. Chem.* **1989**, *161*, 1934.
(10) Kern, R. D.; Chen, H.; Kiefer. J. H.; Mudipali, P. S.*Combust. Flame* **1995**, *100*, 177.
(11) Miller, J. A.; Volponi, J. V.; Pauwels, J. J. *Combust. Flame* **1996**, *105*, 451.
(12) Marinov, N. M.; Pitz, W. J.; Westbrook, C. K.; Castaldi, M. J.; Senkan, S. M. *Combust. Sci. Technol.* **1996**, *116/117*, 211.

(13) Castaldi, M. J.; Marinov, N. M.; Melius, C. F.; Huang, J.-M.; Senkan, S. M.; Pitz, W. J.; Westbrook, C. K. *Symp. (Int.) Combust., [Proc.], 26th* **1996**, *1*, 693.
(14) Miller, J. A. *Symp. (Int.) Combust., [Proc.], 26th* **1996**, *1*, 461.
(15) Lindstedt, R. P.; Skevis, G. *Combust. Sci. Technol.* **1997**, *125*, 73.
(16) Marinov, N. M.; Castaldi, M. J.; Melius, C. F.; Tsang, W. *Combust. Sci. Technol.* **1997**, *128*, 295.
(17) Marinov, N. M.; Pitz, W. J.; Westbrook, C. K.; Vincitore, A. M.; Castaldi, M. J.; Senkan, S. M.; Melius, C. F. *Combust. Flame* **1998**, *114*, 192. Erratum: *Combust. Sci. Technol*. **1998**, *131*.
(18) Slagle, I. R.; Gutman, D. *Symp. (Int.) Combust., 21st* **1986**, 875.
(19) Slagle, I. R.; Gmurczyk, G. W.; Batt, L.; Gutman, D. *Symp. (Int.) Combust., 23rd* **1990**, 115.
(20) Adamson, J. D.; Morter, C. L.; DeSain, J. D.; Glass, G. P.; Curl, R. F. *J. Phys. Chem*. **1996**, *100*, 2125.
(21) Adamson, J. D.; DeSain, J. D.; Curl, R. F.; Glass, G. P. *J. Phys. Chem.* **1997**, *101*, 864.
(22) Morter, C. L.; Domingo, C.; Farhat, S. K.; Cartwright, E.; Glass, G. P.; Curl, R. F. *Chem. Phys. Lett.* **1992**, *195*, 316.
(23) Yuan, L.; DeSain. J. D.; Curl, R. F. *J. Mol. Spectrosc*. **1998**, *187*, 102.
(24) Cartwright, E. L.; Morter, C. L.; Curl, R. F.; Tittel, F. K. *Proc. Int. Conf. Lasers* **1993**, *15*, 857.
(25) Stephens, J. W.; Morter, C. L.; Farhat, S. K.; Glass, G. P.; Curl, R. F. *J. Phys. Chem.* **1993**, *97*, 8944.
(26) Burkholder, J. B.; Howard, C. J.; McKellar, A. R. W.; Vervloet, M. *J. Mol. Spectrosc*. **1990**, *142*, 319.
(27) Raphael, R. A.; Sondheimer, F. *J. Am. Chem. Soc.* **1950**, *72*, 120.
(28) Troe, J. *J. Phys. Chem.* **1979**, *83*, 114.
(29) Gilbert, R. G.; Luther, K.; Troe, J. *Ber. Bunsen-Ges. Phys. Chem.* **1983**, *87*, 169.
(30) This form can be obtained from eq 11 by substituting k_∞ and k_0 for k at the high and low pressures limits, respectively.
(31) Tulloch, J. M.; Macpherson, M. T.; Morgan, C. A.; Pilling, M. J. *J. Phys. Chem.* **1982**, *86*, 3812.
(32) Frisch, M. J.; Trucks, G. W.; Schlegel, H. B.; Scuseria, G. E.; Robb, M. A.; Cheeseman, J. R.; Zakrzewski, V. G.; Montgomery, J. A., Jr.; Stratmann, R. E.; Burant, J. C.; Dapprich, S.; Millam, J. M.; Daniels, A. D.; Kudin, K. N.; Strain, M. C.; Farkas, O.; Tomasi, J.; Barone, V.; Cossi, M.; Cammi, R.; Mennucci, B.; Pomelli, C.; Adamo, C.; Clifford, S.; Ochterski, J.; Petersson, G. A.; Ayala, P. Y.; Cui, Q.; Morokuma, K.; Malick, D. K.; Rabuck, A. D.; Raghavachari, K.; Foresman, J. B.; Cioslowski, J.; Ortiz, J. V.; Stefanov, B. B.; Liu, G.; Liashenko, A.; Piskorz, P.; Komaromi, I.; Gomperts, R.; Martin, R. L.; Fox, D. J.; Keith, T.; Al-Laham, M. A.; Peng, C. Y.; Nanayakkara, A.; Gonzalez, C.; Challacombe, M.; Gill, P. M. W.; Johnson, B. G.; Chen, W.; Wong, M. W.; Andres, J. L.; Head-Gordon, M.; Replogle, E. S.; Pople, J. A. *Gaussian 98*; Gaussian, Inc.: Pittsburgh, PA, 1998.
(33) Raghavachari, K. Private communication, 1999.
(34) Boyd, A. A.; Noziere, B.; Lesclaux, R. *J. Phys. Chem.* **1995**, *99*, 10815.
(35) Steinfeld, J. I.; Francisco, J. S.; Hase, W. L. *Chemical Kinetics and Dynamics*; Prentice-Hall: Englewood Cliffs, NJ, 1989; p 359.